Desalination and Water Treatment
www.deswater.com

doi: 10.5004/dwt.2021.27184

224 (2021) 106–121
June

An experimental and computational investigation of poly(piperazine-amide) thin-film composite membrane for salts separation from water using artificial neural network

Rajesh Mahadeva[a], Romil Mehta[b], Gaurav Manik[a,*], Amit Bhattacharya[b,*]

[a]*Department of Polymer and Process Engineering, Indian Institute of Technology, Roorkee, Uttarakhand, India, Tel. +91-9909030497; email: rmahadeva@pe.iitr.ac.in (R. Mahadeva), Tel. +91-132 2714340; email: gaurav.manik@pe.iitr.ac.in (G. Manik)*
[b]*Membrane Science and Separation Technology Division, Central Salt and Marine Chemicals Research Institute Bhavnagar, Gujarat, India, Tel. +91-7567938978; email: rmlmht@gmail.com (R. Mehta), Tel. +91-278-2567610; email: amit@csmcri.res.in (A. Bhattacharya)*

Received 3 September 2020; Accepted 22 February 2021

ABSTRACT

From ever-evolving techniques for desalination to wastewater treatment, membranes have been established themselves as front runners. Recent advances in the development of thin-film composite (TFC), membranes have enabled efficient contaminant separation in terms of ions as well as organics to improvise water treatment. In this study, poly(piperazine-amide) based three-layer membrane was developed through interfacial polymerization of piperazine (aq.) and 1,3,5-trimesoyl chloride (hexane) on a base polysulfone layer supported on non-woven polyester fabric. Membrane efficiency, in terms of permeate flux and salt rejection, was evaluated experimentally by separating NaCl/Na_2SO_4 from solutions having different salt concentrations (500-20,000 mg/L). The experimental results have been further modeled and simulated using artificial neural network (ANN) trained using efficient algorithms: Levenberg-Marquardt backpropagation (LM-BP), scaled conjugate gradient backpropagation (SCG-BP), and particle swarm optimization (PSO). Modeling performance has been compared using regression coefficient and mean square error. Optimal search of acceleration factors (c_1 = 1.75/1.5, c_2 = 1.75/2.5), weight of inertia (ω = 0.4), swarm size (10), and nodes (10) exhibited superior performance for PSO-ANN model than LM-BP-ANN and SCG-BP-ANN models to enable efficient modeling of output–input correlations. This combined experimental and computational study paves the way for study and development of next-generation TFC membrane materials for desalination and inherent process optimization.

Keywords: Poly(piperazine-amide) thin-film composite membrane; Separation of salts; Artificial neural network; Modeling and simulation; Particle swarm optimization

1. Introduction

1.1. Background and motivation

Water scarcity is an enormous challenge for humans, animals, and plants. However, only a small amount of clean water (~2.5%) present on the earth is available for direct use of human consumption [1,2]. At this time, there is a high inequality between clean water demand and supply, and therefore, around half of the world's population may be stressed by 2030 [1,3]. Hence, various desalination and wastewater treatment techniques have gathered significant attention from academia and the scientific community in the recent era to fulfil the requirement of freshwater globally [4].

Over the years, membrane technology has played an essential role in removing pesticides/salts very effectively

* Corresponding authors.

from contaminated/salted water. The growing global need for freshwater has driven the widespread development of membranes in every aspect, from membrane preparation to its engineering [5–7]. The beauty of membrane research is that it is an active method that moves forward slowly, and in that process, the development of the thin-film composite (TFC) membrane carries immense significance.

The TFC membrane is featured by its network and phenomenally varied with change of constituents in different layers. It is a three-layer composite supported on polyester (non-woven) fabric. The separation and mechanical functions are assigned to different layers of TFC membranes. In this membrane formation, two different steps viz. asymmetric polysulfone membrane and polyamide formation are involved [5,8].

The asymmetric polysulfone membrane is formed by a wet phase separation, which is the most extensively used technique. This happens by the interchange of solvent and non-solvent through the interface between coagulation bath and casting solution. The interfacial polymerization reaction occurs between piperazine ($C_4N_2H_{12}$) and 1,3,5-trimesoyl chloride ($C_9H_3Cl_3O_3$) on asymmetric polysulfone membrane support [5]. An interesting fact of poly(piperazine-amide) membranes is not only its loose network, but also its ability to show selective separation of bivalent over monovalent. This behavior makes it unique and different from poly(1,3-phenylene diamine-amide). In our DFT study, we have tried to explain behavior [7]. The interfacial polymerization is tuned by varying dipping time in monomers (piperazine and trimesoyl chloride) to prepare two different TFC membranes. The separation in terms of monovalent and bivalent salts is marked for these membranes.

Further, a review of modeling and simulation of experimental work has been reported earlier using an advanced learning technique, i.e., artificial neural network (ANN) [4,9,10]. The technique requires no space, cost, instruments, time, and energy as compared to the needs of experimentation. It works very effectively for simple as well as complex datasets, which are more difficult to predict using conventional methods [11–17].

Once the neural network has been modeled, then the subsequent task is to train the network. It may be trained through various training functions/algorithms such as genetic algorithm, artificial bee colony, Levenberg-Marquardt backpropagation (LM-BP), particle swarm optimization (PSO), scaled conjugate gradient backpropagation (SCG-BP) algorithms, imperialist competitive algorithm (ICA), and state vector machine [18]. These training algorithms find the optimum values of various weights (w) and bias (B) of the network.

1.2. Paper organization and contributions

This article has been divided into two main parts: the first one details the experimental setup and analysis (includes materials and methods, analytical techniques, preparation of TFC membrane, filtration experiment, experimental results and discussion) while the other part focuses on details and application of ANN, BP algorithm, PSO method, and their hybrids to effectively model and simulate the membrane behavior for separating chosen salts (NaCl and Na_2SO_4) from water.

The major contributions of this research have been summarized as follows:

- The development of poly(piperazine-amide) based three-layer membrane (Memb-I having low flux and Memb-II having higher flux) through interfacial polymerization of piperazine (aq.) and 1,3,5-trimesoyl chloride (hexane) on a base polysulfone layer supported on non-woven polyester fabric which has the ability to separate salts (NaCl and Na_2SO_4) from water.
- The second contribution is to implement efficient and advanced modeling techniques (LM-BP-ANN, SCG-BP-ANN, and PSO-ANN) to analyze the membrane's behavior observed experimentally. Hence, the performance results show good agreement between simulation and the experimental datasets of the membranes.
- The third contribution is to applied optimization techniques to get best results of membrane performances.

2. Experimental setup

2.1. Materials and methods

The polysulfone (Solvay Advanced Polymers, USA) and non-woven polyester fabric (PGI, France) were used for the support of TFC membrane. Piperazine (Across Organic, USA) and trimesoyl chloride (Sigma-Aldrich, USA) were used for interfacial polymerization. Hexane (Merck, India) and N,N-dimethylformamide (Loba, India) were used as solvents. Separation performances were done using sodium sulfate (Fisher Scientific, India) and sodium chloride (Rankem, India). In the experiment, deionized water has been used for experiments.

2.2. Analytical techniques

The chemical functionalities of poly(piperazine-amide) membranes were evaluated by ATR-FTIR (Agilent Technologies). The surface morphology and topography of the membrane samples were observed through the atomic force microscope (NT-MTD, Russia) and scanning electron microscope (JMS-7100F, Russia). The electrokinetic analyzer (Zeta-CAD, France) with the background electrolyte 1 mM KCl determined the zeta potential of the membranes. The drop shape analyzer (DSA 100, Kruss, Germany) determined the hydrophilicity behavior.

2.3. Preparation of thin-film composite (poly(piperazine-amide) membranes

Polysulfone (15% w/w) solution was made in dimethylformamide at 65°C (150 rpm) for 6 h. Casting of polysulfone-based membrane on the non-woven polyester fabric by wet phase inversion method with the help of prototype casting machine (speed of casting 2 m/min). The interfacial polymerization was carried out between piperazine (in water) and trimesoyl chloride, TMC (in hexane). First, polysulfone-based membrane was dipped (1 min) in piperazine solution after that soaked piperazine membrane

was dipped (1 min) in the TMC solution. As the partition coefficient is high for trimesoyl chloride, the reaction occurred in the hexane phase. The details of the condition are depicted in Table 1 [5].

2.4. Filtration experiment

The filtration experiments were operated at 1.034 MPa with an operative membrane area of 0.00152 m^2. In this, the flow of feed solution was tangential with a cross-flow filtration unit having four stainless cells in series, as shown in Fig. 1. The salts (NaCl and Na_2SO_4) separation was performed with different feed concentrations of 500, 1,000, 2,000, 5,000, 10,000 and 20,000 mg/L. The membrane permeates flux (J_v) and the salt rejection R(%) are determined by Eqs. (1) and (2), respectively.

$$J_v = \frac{Q}{At} \tag{1}$$

where J_v is the membrane permeate flux (L/m^2/h^1), Q is the permeate volume (L), A is the membrane area (m^2), and t is the permeate time (h).

$$R(\%) = \left(1 - \frac{c_p}{c_f}\right) \times 100 \tag{2}$$

where R(%) is the salt rejection, c_p is the permeate concentration (mg/L), and c_f is the feed concentration (mg/L).

3. Model development

3.1. Artificial neural network

Nowadays, ANNs serve as major artificial intelligence tools to promote researchers to solve various engineering as well as medical problems. The developed models are simple, precise, achievable, and can capture the non-linearity of any system. It is an algorithm that mimics the processing in the human brain, is designed to recognize patterns in processes and help to solve technical problems in the system. It has input, hidden, and output layers and every layer may have multiple nodes. ANN receives inputs from input layers while emitting outputs by output layers. However, hidden layers lie between the input and output layers. Fig. 2 illustrates a node, the ANN model's simple processing elements, wherein each node receives a number of inputs from an external source, executes some computation, and produces an output [9,19].

The output of a node (y) is defined through Eq. (3), where x_1, x_2, x_n are the inputs, w_1, w_2, w_n, are the weights, B is the bias, and v is the induced field.

$$y = f(v) = f\left(B + \sum_{j=1}^{n} w_j x_j\right) \tag{3}$$

The inputs of nodes are connected with weights (w_1, w_2, w_n) which are calculated in the training procedure. Bias B has the additional input also associated with nodes and provides constant value to every node. The node employs a function to the weighted sum of its inputs called activation function $f(v)$. It makes non-linearity into the output of a node, as practically datasets are non-linear. In general, logsig, tansig, and purelin are the mostly used activation functions in modeling [4,19,20].

3.2. Modeling strategy

The experimental variables have been divided into input and output variables for the separation of NaCl and Na_2SO_4 from solutions using membranes, Memb-I and Memb-II described earlier. Table 2 illustrates the eight

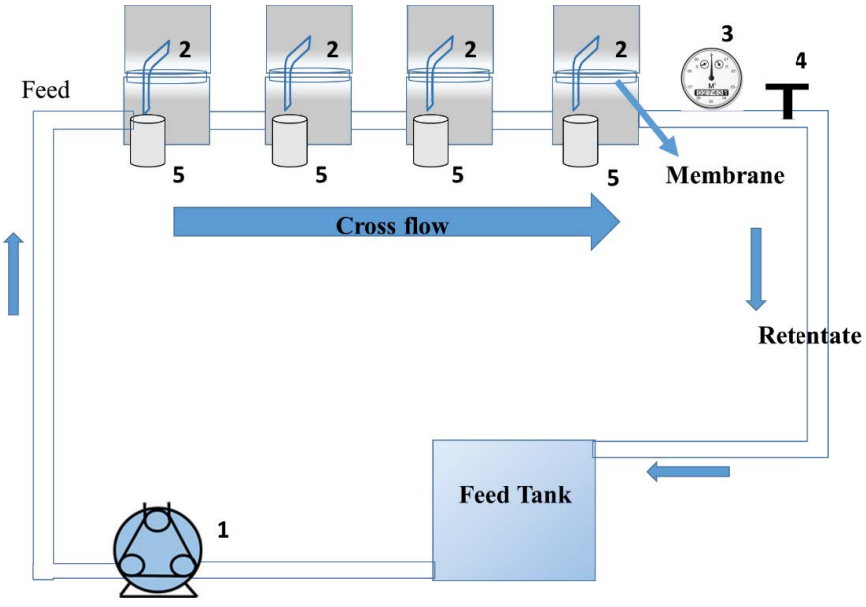

Fig. 1. Graphical representation of an experimental cross-flow filtration unit setup: 1, peristaltic pump; 2, stainless steel separation cell; 3, pressure gauge meter; 4, pressure value, and 5, permeate.

Table 1
Details of interfacial polymerization conditions of TFC membranes (I and II)

TFC membrane	Base membrane	Interfacial polymerization conditions
Memb-I	15% (w/w) polysulfone	PIP, 2% (in water) Dipping time: 2 min TMC, 0.1% (in hexane) Drying: 1 min Curing temperature: 100°C Curing time: 4 min
Memb-II		PIP, 2% (in water) Dipping time: 1 min TMC, 0.1% (in hexane) Drying: 1 min Curing temperature: 100°C Curing time: 4 min

possible combinations of events for the modeling. Every event has been shown a good agreement between experimental and simulation results of the membrane's behavior. However, event number – 4 has been analyzed in detail in this study. The input variables include different salt concentrations (500, 1,000, 2,000, 5,000, 10,000 and 20,000 mg/L), temperature (~25°C), pressure (~1.034 MPa), and pH (~7) and output variables include membrane permeate flux (J_v) in L/m^2/h and salt rejection R(%).

3.3. Implementation of LM-BP-ANN and SCG-BP-ANN models

Training functions play an essential role in the designing of neural networks. In our models, LM-BP and SCG-BP training functions have been used to find optimum process outputs. LM-BP functions use Jacobian derivatives and are faster to implement but require more memory than SCG-BP functions. However, they are not supported on graphics processing unit hardware. SCG-BP functions use gradient derivatives and though they are not as fast as Jacobian backpropagation but they are supported on graphics processing unit hardware with the parallel computing toolbox. BP algorithm has a feedforward connection of layers and each layer feeds successively into the next layers of the system. It provides the system to set inputs with expected outputs over the minimization of mean square error (MSE) chosen as the error function. Table 3 describes the summary of used parameters in LM-BP-ANN and SCG-BP-ANN prediction models.

3.4. Implementation of PSO-ANN models

Kennedy and Russell [21] have invented a stochastic population-based (swarm) search technique called Particle Swarm Optimization (PSO). It is inspired by the social or collective behavior of birds flocking and initialized by a group of random particles. Particles search nearby in a multidimensional space, while each particle corrects its position according to its own best position called *pbest* and another best value obtained by the neighbor particle [22,23]. For finding the best movement velocity and positions of every particle Eqs. (4) and (5) are employed [20,24]. Table 4 describes the summary of the used parameters in the PSO-ANN simulation.

$$v_i^{n+1} = \omega v_i^n + c_1 r_1^n \left[x_{i,p}^n - x_i^n \right] + c_2 r_2^n \left[x_g^n - x_i^n \right] \tag{4}$$

$$x_i^{n+1} = x_i^n + c_i^{n+1} \tag{5}$$

where n is the total number of iterations; i is the particle index; v_i^n and v_i^{n+1} are the particle i velocity at nth and n+1th iteration, respectively; $x_{i,p}^n$ is the individual best position associated with particle i (*pbest*); x_g^n is the global best value, obtained by the particle (*gbest*); c_1, c_2 is the acceleration factors; r_1^n, r_2^n is the random values; x_i^n and x_i^{n+1} are the particle i position at nth and n+1th iteration, respectively; ω is the weight of inertia.

3.5. Evaluation performance indices

To the evaluation of LM-BP-ANN, SCG-BP-ANN, and PSO-ANN based models, regression coefficient (R^2), and MSE have been used as the performance indices. They were computed and analyzed as per the following equations [20]:

$$R^2 = 1 - \frac{\sum_{l=1}^{K} \left(Y_l^{\exp} - Y_l^{\text{pre}} \right)^2}{\sum_{l=1}^{K} \left(Y_l^{\exp} - \overline{Y_l^{\exp}} \right)^2} \tag{6}$$

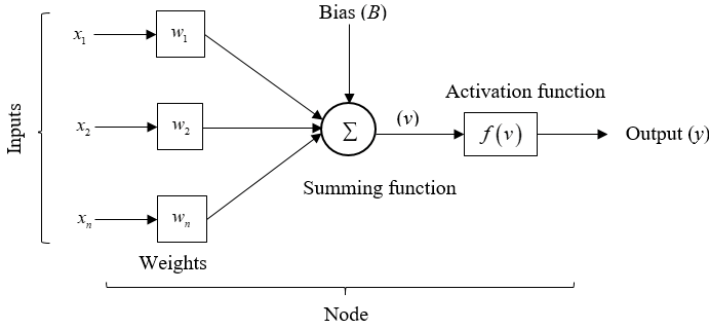

Fig. 2. Simple processing elements of an artificial node of ANN.

Table 2
Modeling strategy of experimental works with an 8 possible combination of events

Events	Input variables	Membrane	Separation of	Output variables
1	(a) Concentration of salts (500, 1,000, 2,000, 5,000, 10,000, and 20,000 mg/L) (b) Temperature (~25°C) (c) Pressure (~1.034 MPa) (d) pH (~7)	Memb-I (having low flux)	NaCl	(1) Permeate flux
2				(2) Rejection
3			Na_2SO_4	(1) Permeate flux
4				(2) Rejection
5		Memb-II (having higher flux)	NaCl	(1) Permeate flux
6				(2) Rejection
7			Na_2SO_4	(1) Permeate flux
8				(2) Rejection

Table 3
Summary of the used parameters in LM-BP-ANN and SCG-BP-ANN prediction models

Models description	Values/comments
Number of input layer and nodes	1 layer and 4 nodes
Number of hidden layer and nodes	1 layer (nodes vary)
Number of output layer and nodes	1 layer and 2 nodes
Number of datasets for training	120 × 5 = 600
Datasets divided for training	Training (75%), validation (15%), and testing (15%)
Maximum iterations	1,000
Training functions	LM-BP and SCG-BP
Operating tool	Neural network toolbox MATLAB-R2019b
System configuration	Intel (R) Core (TM) i5-8250U CPU @ 1.60 GHz, 4 Core(s), 1801 MHz, 8 Logical processors, 8.00 GB RAM

where K is the number of training or validation or testing samples, $Y_l^{\exp}$ is the experimental data, Y_l^{pre} is the predicted data, and $\overline{Y_l^{\exp}}$ is the mean of experimental data.

$$\text{MSE} = \frac{1}{K}\sum_{l=1}^{K}\left(Y_l^{\exp} - Y_l^{\text{pre}}\right)^2 \tag{7}$$

where K is the number of training or validation or testing samples, $Y_l^{\exp}$ is the experimental data, and Y_l^{pre} is the predicted data.

4. Results and discussion

4.1. Membrane characterization

The ATR-FTIR spectra (Fig. 3) analysis of the TFC membranes (I and II) show a similar absorption band 1,626 cm^{-1} (carboxylic acid and amide), 1,443 cm^{-1} assigned to poly(piperazine-amide) on the polysulfone base membrane.

Fig. 4 illustrates the surface morphology of TFC membranes (I and II). Memb-I shows a better density of disperse particles as compared to Memb-II. EDAX analysis results depict the relatively low nitrogen percentage of Memb-II as compared to Memb-I. Atomic force micrograph (AFM) analysis of membranes (Fig. 5) shows that the roughness of poly(piperazine-amide) increases in comparison to the polysulfone membrane. It suggests that with coating increased

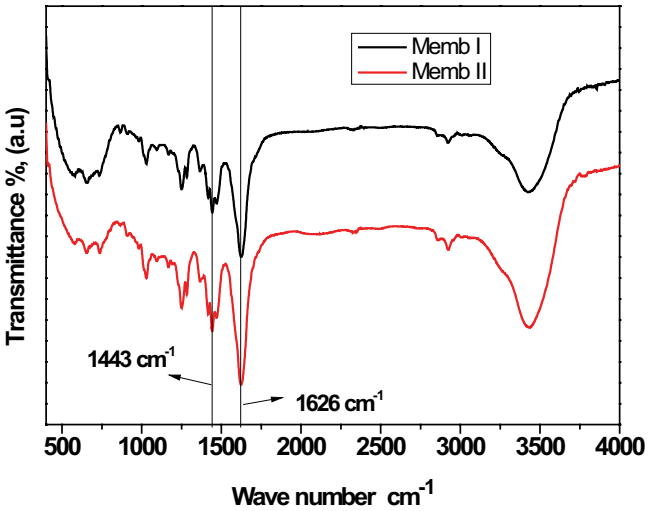

Fig. 3. ATR-FTIR analysis of TFC membranes (I and II).

the roughness increases because of poly(piperazine-amide) moiety attached to the surface. Additionally, the contact angles of water droplets captured show that membranes (I and II) have gained hydrophilic property (contact angle 52° and 48°, respectively) due to coating of poly(piperazine-amide) on the polysulfone membrane which is relatively

Table 4
Summary of the used parameters in PSO-ANN (swarm size 5, 10, 15, and 20) model

PSO-ANN description	Values/comments
Number of input layer and nodes	1 layer and 4 nodes
Number of hidden layer and nodes	1 layer (nodes vary)
Number of output layer and nodes	1 layer and 2 nodes
Activation function (hidden layer)	Logsig
Activation function (output layer)	Purelin
Number of datasets for training	120 × 5 = 600
Maximum iterations	1,000
c_1 and c_2	1.5 and 2.5
Number of particles (swarm size)	5, 10, 15, and 20
Upper and lower bound of variables	+1.5 and −1.5
Objective function	$\sum$((net (inputs)-targets)^2)/length (inputs)
Operating tool	Neural network toolbox MATLAB-R2019b
System configuration	Intel (R) Core (TM) i5-8250U CPU @ 1.60 GHz, 4 Core(s), 1,801 MHz, 8 Logical processors, 8.00 GB RAM

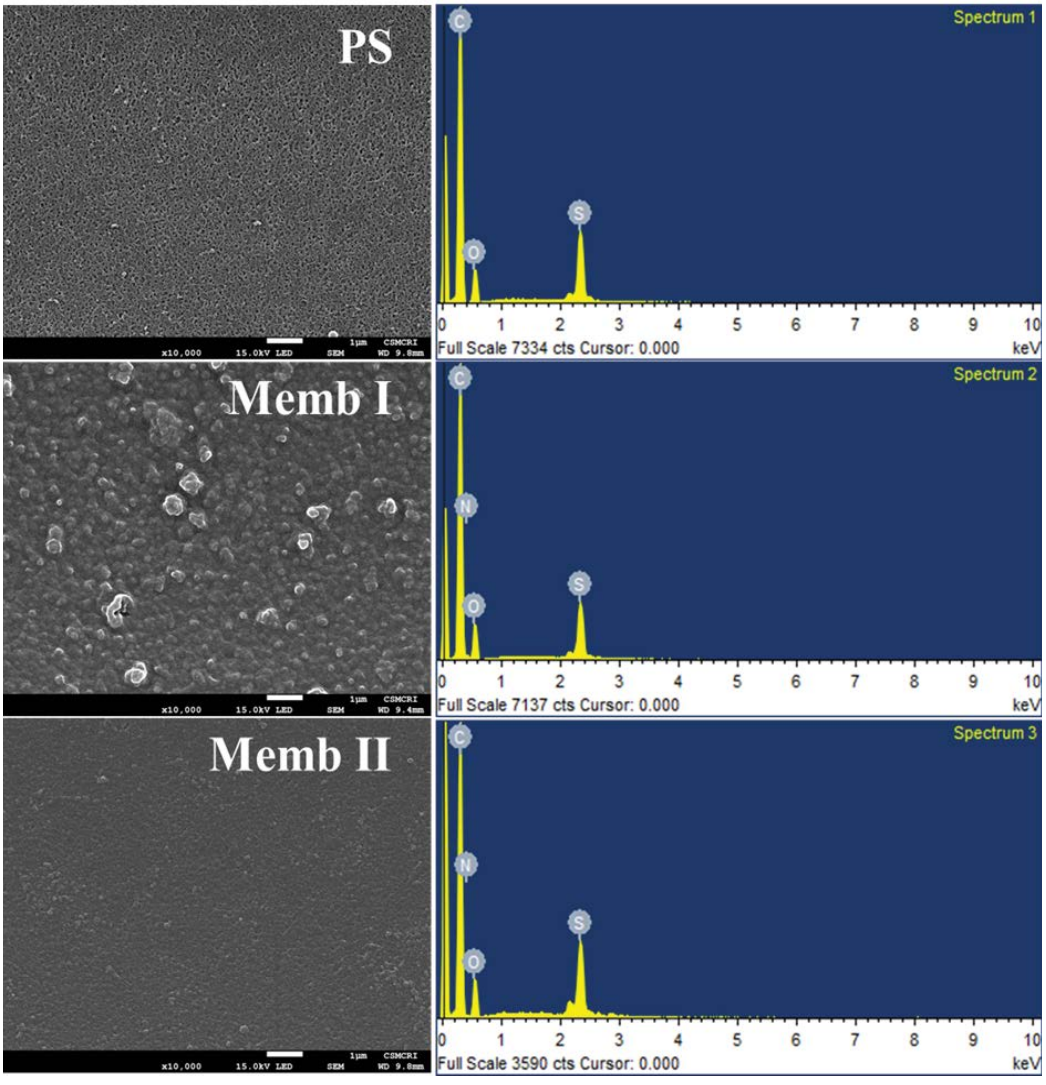

Fig. 4. Scanning electron micrograph and EDAX analysis of membranes (I and II).

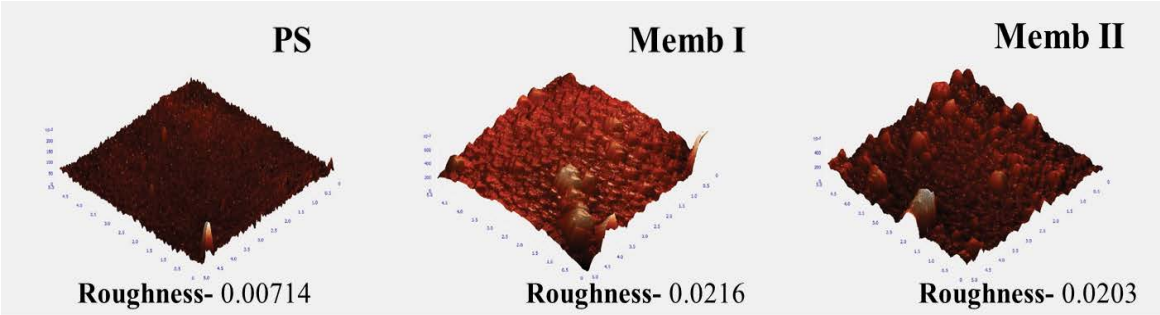

Fig. 5. Atomic force micrograph (AFM) of membranes (I and II).

hydrophobic (contact angle 72°) one. The zeta potential of Memb-I and Memb-II shows −16.98 and −21.08 mV, respectively. Memb-II gives more negative charge because amine monomer and acid chloride monomer reaction time is less so the presence of free –COOH group is more.

The permeate flux showed dependence on the dipping time of monomers of interfacial polymerization. Water flux was observed to decrease with the increasing feed salt concentration as the elevated osmotic pressure reduces the net applied pressure. Memb-II due to mentioned characteristics demonstrated more permeate flux than Memb-I.

4.2. Salts separation performances

The monovalent ion (NaCl) and bivalent ion (Na_2SO_4) separation performances for Memb-I and Memb-II are shown in Tables 5 and 6, respectively. The separation performances of bivalent ion over monovalent ion by the poly(piperazine-amide) membrane are already reported [6,25]. The permeate flux of Memb-II was more for the Memb-I because of the interfacial polymerization reaction time and the resultant poly(piperazine-amide) layer formation was more. Another observation was that increasing the salt concentration (500–20,000 mg/L), the membrane flux and rejection of salts decreased. The rejection of the Na_2SO_4 was more than the NaCl because of charge, size, and diffusion coefficient difference (size and diffusion coefficient of Cl^- ion 0.12 nm/2.03 × 10^{-9} m^2/s and SO_4^{2-} ion 0.23 nm/1.06 × 10^{-9} m^2/s) [26,27].

4.3. Simulation results and discussions

4.3.1. LM-BP-ANN model simulated results

Table 7 describes the performance results (R^2 and MSE) of the LM-BP-ANN model. In this model, input variables include different salt concentrations (500, 1,000, 2,000, 5,000, 10,000, and 20,000 mg/L), temperature (~25°C), pressure (~1.034 MPa), and pH (~7) and output variables include salt rejection R(%) (Na_2SO_4) from Memb-I. Twelve models (LM-1 to LM-12) have been analyzed with different combinations of nodes in the hidden layer of ANN. Datasets have been divided into training (70%), validation (15%), and testing (15%). Among different models simulated, model LM-1 has performed the best for validation (R^2 = 0.9131, MSE = 1.2767) with a single chosen node and a single hidden layer, but overall validation performance was different for different nodes in the hidden layer. Model LM-6 has been considered for data analysis. Fig. 6 illustrates the regression plot of the LM-BP-ANN model. However, validation (15%) gave the best regression coefficient (R^2 = 0.8473) in this model. Fig. 7 shows the MSE using 10 nodes in the hidden layer of this model. Validation achieved superior performance (MSE = 1.0414) at 2 epoch compared to training and testing. Fig. 8 displays the error histogram with a 20 bin size of the LM-BP-ANN model using 10 nodes in the hidden layer. It accounts for errors histogram with training, validation, and testing with different instances.

4.3.2. SCG-BP-ANN model simulated results

Simulation results (R^2 and MSE) of an optimal architecture using the SCG-BP-ANN model are shown in Table 8. Model SCG-5 with 8 nodes in the hidden layer of ANN gave the best performance with R^2 = 0.8434 and MSE = 1.5631 for training. Model SCG-6 has been considered for data analysis. Fig. 9 shows the regression plot of the SCG-BP-ANN model (training (70%), validation (15%), testing (15%), and all datasets (100%) using 10 hidden layer nodes). However, validation performed best regression coefficient (R^2 = 0.8797) in this model. Fig. 10 illustrates the MSE using 10 nodes in the hidden layer of ANN. The best performance of validation (MSE = 1.0658) at 23 epoch. LM-BP-ANN (2 epoch) has a faster response than SCG-BP-ANN (23 epoch). Error histogram with a 20 bin size of the SCG-BP-ANN model using 10 nodes in the hidden layer is shown in Fig. 11 with various instances.

4.3.3. PSO-ANN (swarm size 5, 10, 15, and 20) models simulated results

PSO algorithms performed as the best training function support to the neural network as observed from Table 9. Different models with various combinations of nodes in the hidden layer of ANN shows the performance results in the form of the regression coefficient (R^2) and MSE. The performance of PSO algorithms depends upon the swarm size, acceleration factors (c_1 and c_2), and weight of inertia (ω). Here, PSO-ANN models have been analyzed with swarm sizes 5, 10, 15, and 20. PSO-ANN (swarm size 5) model has more variations than PSO-ANN (swarm size 10, 15, and 20). Modeling and simulation involves input variables as different salt concentrations (500, 1,000, 2,000, 5,000, 10,000, and

Table 5
Salts (NaCl and Na_2SO_4) separation performances through Memb-I

Salt concentration (mg/L)	Memb-I			
	NaCl		Na_2SO_4	
	Flux (L/m²/h)	Rejection (%)	Flux (L/m²/h)	Rejection (%)
500	41.1	64.1	45.1	96.8
1,000	41.2	59.6	44.6	96.9
2,000	40.9	53.9	43.9	96.4
5,000	40.5	45.8	42.2	94.8
10,000	34.8	36.6	38.8	93.7
20,000	32.6	30.8	31.9	91.9

Table 6
Salts (NaCl and Na_2SO_4) separation performances through Memb-II

Salt concentration (mg/L)	Memb-II			
	NaCl		Na_2SO_4	
	Flux (L/m²/h)	Rejection (%)	Flux (L/m²/h)	Rejection (%)
500	64.4	65.5	61.9	96.8
1,000	63.4	64.5	61.1	96.1
2,000	62.6	57.1	60.2	95.5
5,000	61.4	45.3	58.8	95.2
10,000	54.9	37.1	53.7	94.4
20,000	50.1	32.5	48.7	91.9

Table 7
Simulation results of an optimal architecture using the LM-BP-ANN model

Model No.	Number of nodes	Performance results of chosen data							
		Training (70%)		Validation (15%)		Testing (15%)		All (100%)	
		R^2	MSE	R^2	MSE	R^2	MSE	R^2	MSE
LM-1	1	0.7867	1.8382	0.9131	1.2767	0.8669	1.2019	0.8213	1.6576
LM-2	2	0.8327	1.5648	0.8851	1.0882	0.7345	2.7457	0.8208	1.6705
LM-3	4	0.8254	1.3626	0.7617	3.4056	0.8962	1.2570	0.8222	1.6532
LM-4	6	0.8562	1.4552	0.7841	1.9888	0.7094	2.4232	0.8207	1.6804
LM-5	8	0.8192	1.5149	0.8060	2.8984	0.8704	1.1395	0.8203	1.6661
LM-6	**10**	**0.7985**	**1.7012**	**0.8473**	**1.0414**	**0.7282**	**4.1952**	**0.7879**	**1.9763**
LM-7	12	0.8276	1.7130	0.8633	0.8736	0.7305	2.1310	0.8222	1.6498
LM-8	14	0.8068	1.8514	0.8260	1.3807	0.8971	0.9558	0.8215	1.6465
LM-9	16	0.8084	1.7301	0.8830	1.9075	0.8393	1.1277	0.8203	1.6664
LM-10	18	0.8376	1.7249	0.7037	2.4669	0.7600	1.4854	0.8078	1.8820
LM-11	20	0.8417	1.4260	0.7958	1.5130	0.7358	2.9269	0.8194	1.6442
LM-12	25	0.7896	1.8845	0.8760	0.9739	0.9054	1.3167	0.8202	1.6627

Salt to be separated: Na_2SO_4; process parameter evaluated: salt rejection R(%); membrane used: Memb-I (low flux membrane); training function used: Levenberg-Marquardt backpropagation (LM-BP); datasets division: training 70%, validation 15%, and testing 15%; number of hidden layers: 1.

20,000 mg/L), temperature (~25°C), pressure (~1.034 MPa), and pH (~7) and output variable salt rejection R(%) (Na_2SO_4) from Memb-I. Table 9 shows that, among various models for different nodes (1–25), two models (model PSO-3 and PSO-6) provided the best performance (R^2 = 0.8280, MSE = 1.5886) for 4 and 10 nodes in hidden layer of ANN, respectively, and using swarm size of 10. In general, the regression coefficient (R^2) of PSO-ANN models is better than those of LM-BP-ANN

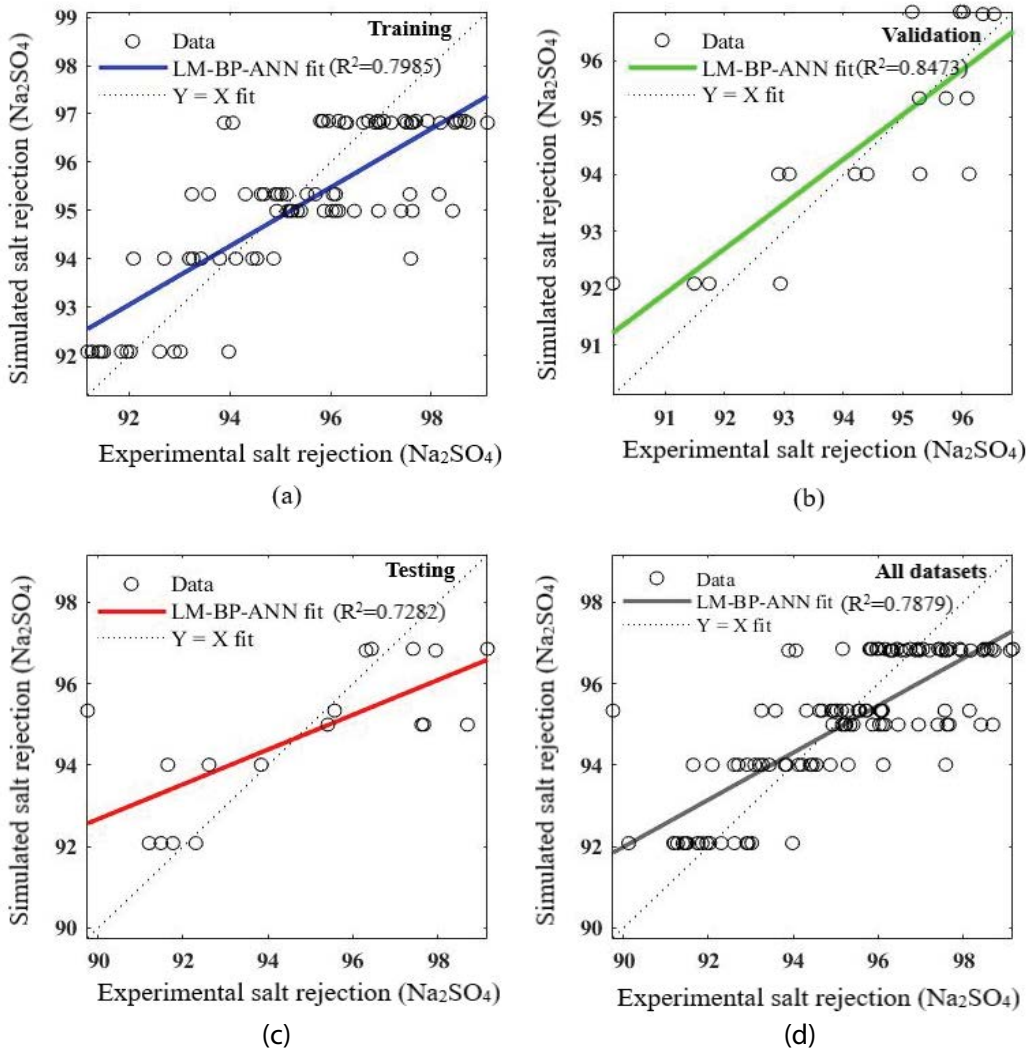

Fig. 6. Regression plot of LM-BP-ANN model using 10 nodes in hidden layer for model LM-6: (a) training (70%), (b) validation (15%), (c) testing (15%), and (d) all datasets (100%).

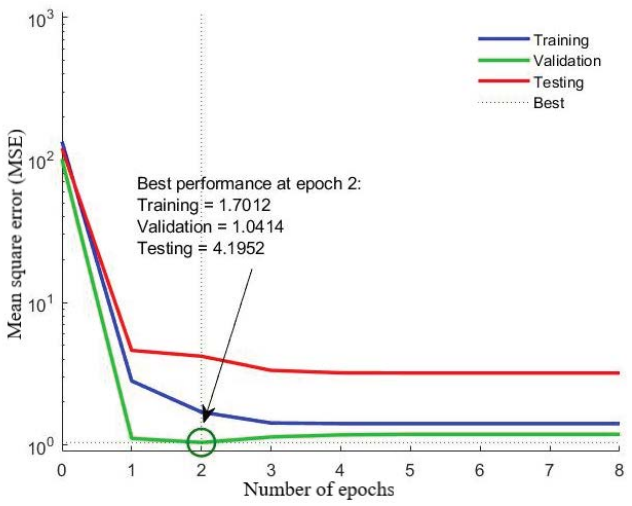

Fig. 7. Mean square error (MSE) of LM-BP-ANN model using 10 nodes in the hidden layer for model LM-6.

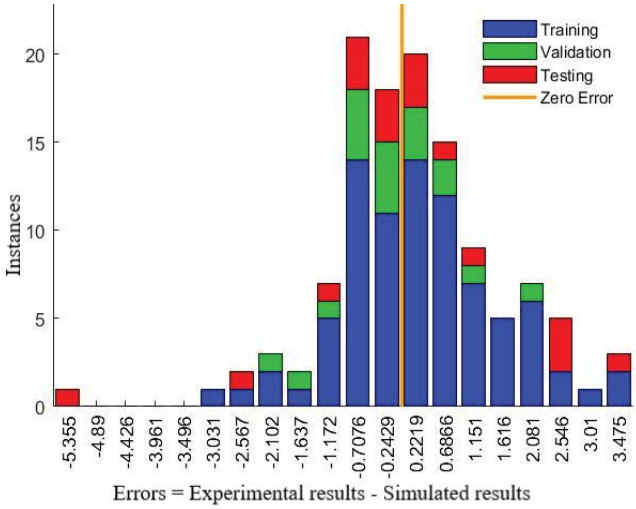

Fig. 8. Error histogram with 20 bin of the LM-BP-ANN model using 10 nodes in the hidden layer for the model LM-6.

Table 8
Simulation results of an optimal architecture using the SCG-BP-ANN model

Model No.	Number of nodes	Performance results of chosen data							
		Training (70%)		Validation (15%)		Testing (15%)		All (100%)	
		R^2	MSE	R^2	MSE	R^2	MSE	R^2	MSE
SCG-1	1	0.7772	2.1944	0.8752	0.9881	0.8014	1.4839	0.7893	1.9068
SCG-2	2	0.8127	1.7357	0.7730	1.6385	0.8917	1.2581	0.8212	1.6495
SCG-3	4	0.7894	2.0587	0.7489	1.7438	0.9133	0.8633	0.8012	1.8321
SCG-4	6	0.7920	1.9337	0.8798	1.1976	0.8713	1.0493	0.8158	1.6907
SCG-5	8	0.8434	1.5631	0.7072	2.2638	0.8723	1.0005	0.8239	1.6378
SCG-6	**10**	**0.8190**	**1.5813**	**0.8797**	**1.0658**	**0.7935**	**2.6270**	**0.8219**	**1.6608**
SCG-7	12	0.7970	1.7772	0.8765	1.5160	0.8696	1.2184	0.8203	1.6542
SCG-8	14	0.8101	1.8091	0.9434	0.5502	0.7580	2.1868	0.8178	1.6769
SCG-9	16	0.8399	1.6594	0.6952	1.8924	0.7399	1.8140	0.8145	1.7175
SCG-10	18	0.8402	1.5484	0.8118	1.2827	0.7460	2.5906	0.8211	1.6449
SCG-11	20	0.7884	1.8938	0.8782	1.2590	0.9171	0.8360	0.8221	1.6399
SCG-12	25	0.8374	1.5960	0.8062	1.6093	0.7346	1.8073	0.8232	1.6297

Salt to be separated: Na_2SO_4; process parameter evaluated: salt rejection R(%); membrane used: Memb-I (low flux membrane); training function used: scaled conjugate gradient backpropagation (SCG-BP); datasets division: training 70%, validation 15%, and testing 15%; number of hidden layers: 1.

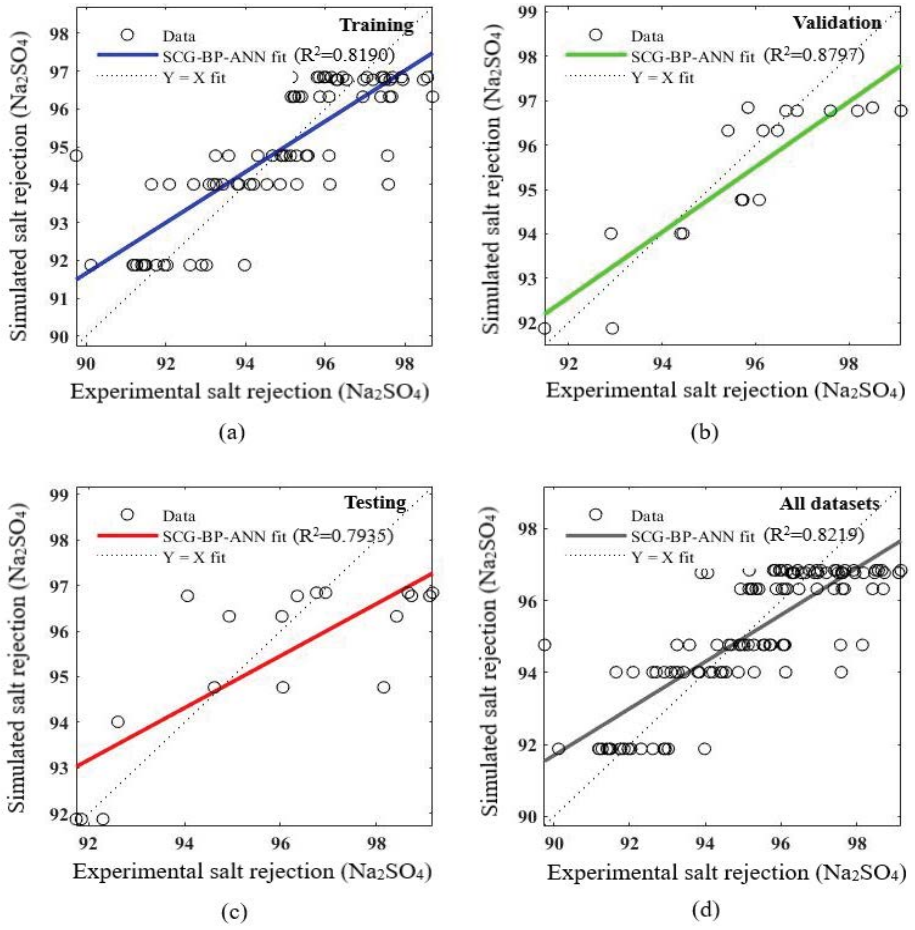

Fig. 9. Regression plot of SCG-BP-ANN model using 10 nodes in hidden layer for model SCG-6: (a) training (70%), (b) validation (15%), (c) testing (15%), and (d) all datasets (100%).

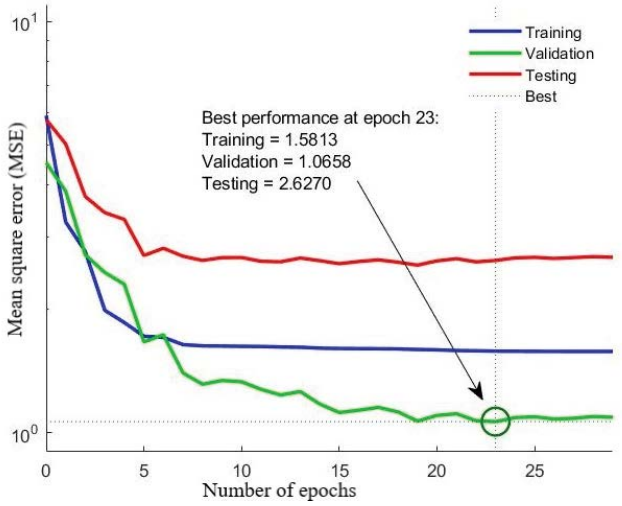

Fig. 10. MSE of the SCG-BP-ANN model using 10 nodes in the hidden layer for model SCG-6.

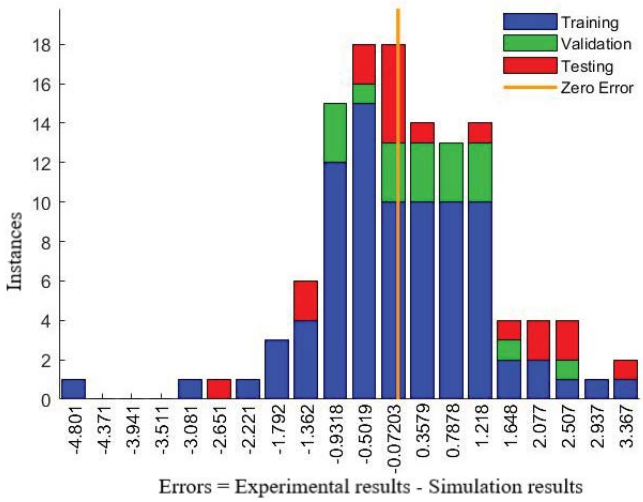

Fig. 11. Error histogram with 20 bin of the SCG-BP-ANN model using 10 nodes in the hidden layer for model SCG-6.

Table 9
Simulation results of an optimal architecture using the PSO-ANN (swarm size 5, 10, 15, and 20) model

Model No.	Number of nodes	Performance results of chosen data							
		Swarm size (5)		Swarm size (10)		Swarm size (15)		Swarm size (20)	
		R^2	MSE	R^2	MSE	R^2	MSE	R^2	MSE
PSO-1	1	0.8166	1.8218	0.8261	1.6045	0.8262	1.6045	0.8253	1.6117
PSO-2	2	0.8269	1.5984	0.8278	1.5910	0.8270	1.5972	0.8272	1.5953
PSO-3	**4**	0.8264	1.6029	**0.8280**	**1.5886**	0.8260	1.6062	0.8279	1.5902
PSO-4	6	0.8138	1.7123	0.8275	1.5932	0.8277	1.5915	0.8274	1.5942
PSO-5	8	0.8268	1.5990	0.8270	1.5973	0.8278	1.5904	0.8272	1.5959
PSO-6	**10**	0.8203	1.6540	**0.8280**	**1.5886**	0.8278	1.5904	0.8272	1.5956
PSO-7	12	0.8240	1.6247	0.8231	1.6342	0.8273	1.5947	0.8271	1.5969
PSO-8	14	0.8268	1.5993	0.8272	1.6013	0.8270	1.5971	0.8270	1.5977
PSO-9	16	0.8275	1.5933	0.8268	1.5990	0.8281	1.5878	0.8279	1.5899
PSO-10	18	0.8263	1.6033	0.8278	1.5906	0.8264	1.6033	0.8280	1.5890
PSO-11	20	0.8256	1.6093	0.8275	1.5933	0.8276	1.5922	0.8276	1.5924
PSO-12	25	0.8173	1.7323	0.8248	1.6175	0.8204	1.6549	0.8253	1.6152

Salt to be separated: Na_2SO_4; process parameter evaluated: salt rejection R(%); membrane used: Memb-I (low flux membrane); training function used: particle swarm optimization (PSO-ANN); c_1 and c_2: 1.5 and 2.5; swarm size: 5, 10, 15, and 20; number of hidden layers: 1.

and SCG-BP-ANN models. Fig. 12 illustrates the regression plot using PSO-ANN (swarm size 10) model with 10 nodes in the hidden layer (model PSO-6 has been considered for data analysis). Fig. 13 demonstrated the MSE using PSO-ANN (swarm size 10) model with 10 nodes in the hidden layer. It shows almost saturation of results beyond iterations.

Armaghani et al. [28] developed PSO-ANN and ICA-ANN prediction models for assessing the tunnel boring machine performance. He described the effects of acceleration factors (c_1 and c_2) used in the PSO-ANN model on the system. Table 10 describes the effects of c_1 and c_2 on PSO-ANN results with swarm size of 10 and 10 nodes in the hidden layer. Model AF-9 and AF-11 gave the best performance with $c_1 = c_2 = 1.75$ and $c_1 = 1.5$, $c_2 = 2.5$, respectively. However, model AF-7 underperformed with the lowest R^2 (0.7855) and highest MSE (1.9793) with $c_1 = c_2 = 2.5$.

Weight of inertia (ω) is an important parameter in the PSO algorithm, which may significantly, affect the process modeling. In the literature, a large variation in weight of inertia (ω) employed has been observed for various applications [29–31]. Table 11 describes the effect of the weight of inertia (ω) on the PSO-ANN model with swarm size of 10 and 10 nodes in the hidden layer of ANN. Model ω-6 displayed the best performance (R^2 = 0.8281, MSE = 1.5884)

with weight of inertia (ω = 0.4). Thus, the above simulation results indicate that the modeling parameters play an essential role in the membrane's performance.

4.3.4. Comparison analysis of LM-BP-ANN, SCG-BP-ANN, and PSO-ANN models

This study has modeled and simulated event number – 4 (Memb-I having low flux for the rejection of Na_2SO_4) using advanced learning techniques (LM-BP-ANN, SCG-BP-ANN, and PSO-ANN models) in detail. The modeling performances have been evaluated with the regression coefficient and MSEs. As a result, we have observed that simulated outputs have been performed almost similar to the experimental datasets of the membrane's behaviors. Fig. 14 illustrates a comparison analysis of the techniques mentioned above with the number of nodes in the hidden layer of ANN. Besides, LM-BP-ANN and SCG-BP-ANN models show more variation than PSO-ANN (swarm size 10) models as a function of a different number of nodes chosen. PSO-ANN (swarm size 10) has achieved continuously stable outcomes of the membrane parameters with the varying number of nodes in the hidden layer of ANN. Likewise, Fig. 15 shows the comparative analysis of MSE of LM-BP-ANN, SCG-BP-ANN, and PSO-ANN (swarm size 10) models. PSO-ANN models have much

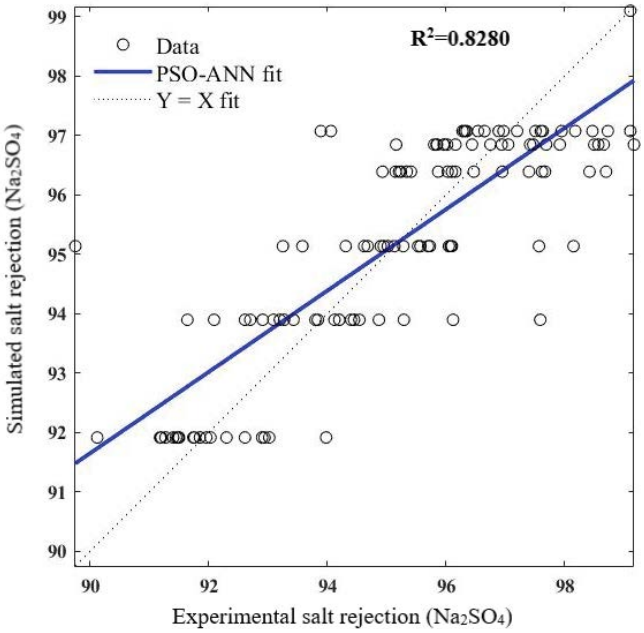

Fig. 12. Regression plot using PSO-ANN (swarm size 10) model with 10 nodes in the hidden layer for model PSO-6.

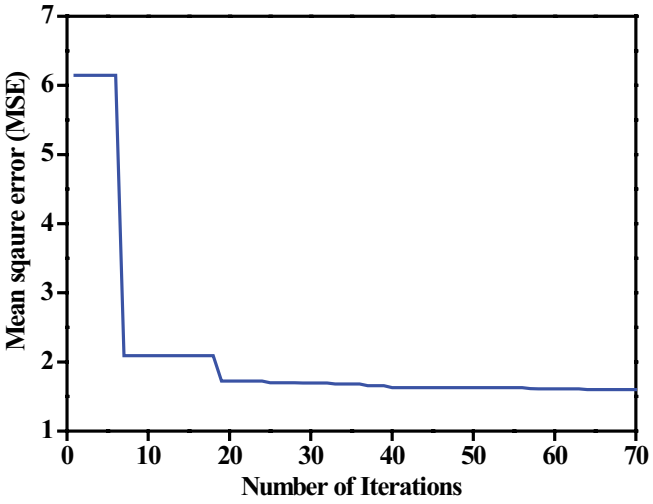

Fig. 13. Mean square error (MSE) using PSO-ANN (swarm size 10) model with 10 nodes in the hidden layer for model PSO-6.

Table 10
Various effects of acceleration factors (c_1 and c_2) using PSO-ANN (swarm size 10) model

Model No.	Number of nodes	Swarm size	c_1	c_2	Performance parameters	
					R^2	MSE
AF-1	10	10	0.8	3.2	0.8279	1.5903
AF-2	10	10	1.333	2.667	0.8162	1.6885
AF-3	10	10	1.714	2.286	0.8246	1.6176
AF-4	10	10	3.2	0.8	0.8248	1.6366
AF-5	10	10	2.667	1.333	0.8264	1.6727
AF-6	10	10	2.286	1.714	0.8277	1.5919
AF-7	**10**	**10**	**2.5**	**2.5**	**0.7855**	**1.9793**
AF-8	10	10	2	2	0.8278	1.5910
AF-9	10	10	1.75	1.75	0.8280	1.5886
AF-10	10	10	1.5	1.5	0.8221	1.6385
AF-11	**10**	**10**	**1.5**	**2.5**	**0.8280**	**1.5886**
AF-12	10	10	1.25	1.25	0.8123	1.7206
AF-13	10	10	1	1	0.8270	1.5973

Salt to be separated: Na_2SO_4; process parameter evaluated: salt rejection R(%); membrane used: Memb-I (low flux membrane); training function used: particle swarm optimization (PSO-ANN); c_1 and c_2: varied; swarm size: 10; number of hidden layers: 1.

Table 11
Effect of weight of inertia (ω) on the PSO-ANN model (swarm size 10)

Model No.	Number of nodes	Swarm size	Weight of inertia (ω)	Performance parameter	
				R^2	MSE
ω-1	10	10	0.05	0.8180	1.6908
ω-2	10	10	0.1	0.8275	1.5936
ω-3	10	10	0.2	0.8280	1.5886
ω-4	10	10	0.25	0.8280	1.5887
ω-5	10	10	0.3	0.8280	1.5889
ω-6	**10**	**10**	**0.4**	**0.8281**	**1.5884**
ω-7	10	10	0.5	0.8276	1.5928
ω-8	10	10	0.6	0.8147	1.7280
ω-9	10	10	0.7	0.8278	1.5921
ω-10	10	10	0.75	0.8069	1.7951
ω-11	10	10	0.8	0.8181	1.6769
ω-12	10	10	0.9	0.8217	1.6752
ω-13	10	10	1	0.8126	1.7569
ω-14	10	10	0.1+rand*0.4	0.8280	1.5886

Salt to be separated: Na_2SO_4; process parameter evaluated: salt rejection R(%); membrane used: Memb-I (low flux membrane); training function used: particle swarm optimization (PSO-ANN); c_1 and c_2: 1.5 and 2.5; swarm size: 10; number of hidden layers: 1.

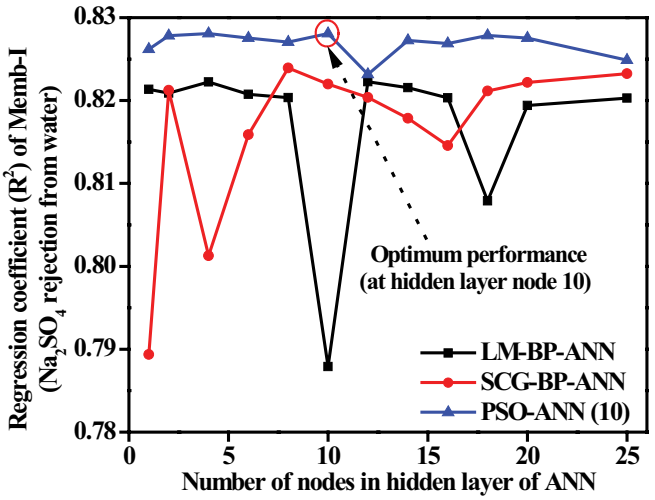

Fig. 14. Performance analysis of models LM-BP-ANN, SCG-BP-ANN, and PSO-ANN (swarm size 10) using regression coefficients (R^2) for Memb-I (low flux membrane) for Na_2SO_4 rejection.

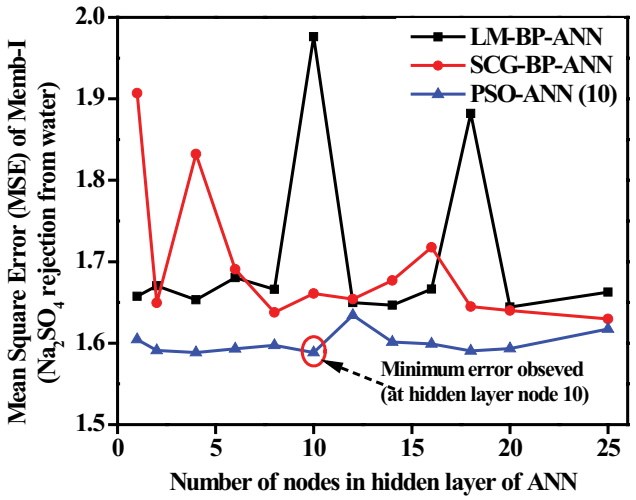

Fig. 15. Performance analysis of models LM-BP-ANN, SCG-BP-ANN, and PSO-ANN (swarm size 10) mean square error (MSE) for Memb-I (low flux membrane) for Na_2SO_4 rejection.

less MSE than LM-BP-ANN and SCG-BP-ANN models. It is also observed that PSO-ANN model results have less deviation than LM-BP-ANN and SCG-BP-ANN models.

Based on the preceding simulated results and discussion of Memb-I (having low flux) for the rejection of Na_2SO_4 from water, we have modeled and simulated Memb-II (having higher flux) for the rejection of Na_2SO_4 from water. The parameters (c_1 = 1.5, c_2 = 2.5, ω = 0.4, training activation function = trainlm, trainscg, swarm size = 10) have been used for the modeling. Figs. 16 and 17 illustrate the performance analysis of models LM-BP-ANN, SCG-BP-ANN, and PSO-ANN (swarm size 10) for Memb-II having high flux using regression coefficients (R^2) and MSE, respectively.

In addition, the simulation results for event – 2 for NaCl rejection with low flux (Memb-I) have been presented in Figs. S1 and S2 to understand the model performance for NaCl separation as well. The model simulation results to the case of NaCl rejection again show good agreement of simulation with experimental datasets. Besides, Na_2SO_4 rejection from water simulation results performed better than NaCl rejection.

We have observed that the PSO-ANN model has performed the best results than LM-BP-ANN and SCG-BP-ANN techniques. In addition, it has been noticed that the Memb-II (having high flux) increased the regression coefficient than the Memb-I (having low flux) for the rejection of Na_2SO_4.

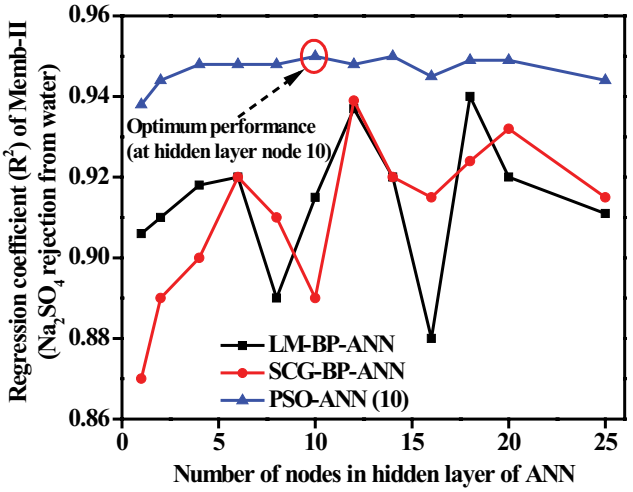

Fig. 16. Performance analysis of models LM-BP-ANN, SCG-BP-ANN, and PSO-ANN (swarm size 10) using regression coefficients (R^2) for Memb-II (high flux membrane) for Na_2SO_4 rejection.

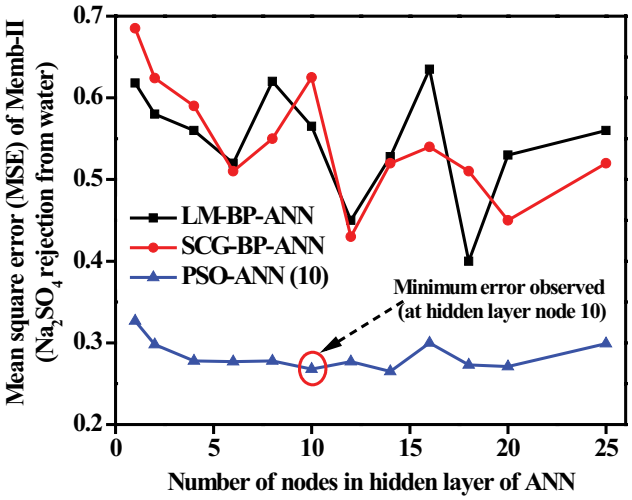

Fig. 17. Performance analysis of models LM-BP-ANN, SCG-BP-ANN, and PSO-ANN (swarm size 10) mean square error (MSE) for Memb-II (high flux membrane) for Na_2SO_4 rejection.

AFM analysis of membranes (Fig. 5) shows that the roughness of Memb-I (0.0216) is more than the roughness of Memb-II (0.0203). Simulation results show that the high roughness membrane (Memb-I) shows relatively less regression coefficients. The results, hence, suggest that roughness may affect the model simulation performance of the membranes. Additionally, the models performed better (low MSE) with the membrane (Memb-II) with a low contact angle (48°) than the other (Memb-I) with high contact angle (52°), indicating that ANN-based models show superior modeling with membranes with higher hydrophilicity.

Our analysis confirms the performance results obtained previously by several researchers and scientists. For instance, it has been found likewise that PSO-ANN models have been found to be superior in adjusting the synaptic weights of ANN than BP-ANN models [20,32–34]. However, it may also depend upon the swarm sizes (5, 10, 15, and 20), acceleration factors (c_1 and c_2), and weight of inertia (ω). The medium swarm sizes are found to be suitable for the best system performances, though it may also depend upon the used experimental datasets. Our performance results of acceleration factors c_1 = 1.75/1.5, c_2 = 1.75/2.5 strongly agree to the earlier findings by Aryafar et al. [35] that "$c_1 + c_2 \leq 4$ must be satisfied for better results". Besides, our best performance results observed with the weight of inertia ω = 0.4, found in the range also confirm to the earlier works by Khajeh et al. [29] (ω = 0.05, 0.1), Buyukyildiz et al. [30] (ω = 0.4, 0.9), and Khajeh et al. [31] (ω = 0.05, 0.6, 0.1, 0.8) and enforce the fact that the weight of inertia (ω) in the range of 0.05–1.0 for such systems helps to achieve best ANN modeling results.

5. Conclusion

Poly(piperazine-amide) TFC membranes (I and II) were prepared for the separation of monovalent and bivalent salts from water. It is a three-layer composite supported on polyester (non-woven) fabric. The separation and mechanical functions are assigned to different layers of TFC membranes. In this membrane formation, two different steps, viz. asymmetric polysulfone membrane, polyamide formation, are involved. The experimental datasets have been simulated using ANN that is the most suitable and applicable simulation technique for water purification and desalination. Six models based on LM-BP-ANN, SCG-BP-ANN, and PSO-ANN (swarm size 5, 10, 15, and 20) have been developed for the optimization of results. Neural network has been modeled with four experimental inputs including concentration of salts (500, 1,000, 2,000, 5,000, 10,000, and 20,000 mg/L), temperature (~25°C), pressure (~1.034 MPa), and pH (~7). Two experimental outputs include membrane permeate flux (J_v) in L/m²/h and salt rejection R(%). Simulated performance results have been evaluated by regression coefficients (R^2) and MSE.

Feature of poly(piperazine-amide) membranes is not only its loose network, but also its selective separation of bivalents over monovalent. Memb-I (lower flux) displayed a better density of dispersed particles compared to Memb-II (higher flux). Contact angles of water droplets show that membranes (I and II) have gained hydrophilic property (contact angle 52° and 48°, respectively) due to the coating of poly(piperazine-amide) on the polysulfone membrane (hydrophobic with contact angle 72°). Zeta potential of membranes (I and II) was found to be −16.98 and −21.08 mV, respectively. Memb-II gives more negative charge because of amine monomer and as acid chloride monomer reaction time is less, so the presence of free –COOH group is more. The permeate flux was found to be dependent on the dipping time of monomers of interfacial polymerization. Hence, Memb-I with higher dipping time than Memb-II displayed less permeate flux than Memb-II.

The comparison of modeling performance among simulated six models using R^2 and MSE indicated that PSO-ANN model (verses LM-BP-ANN and SCG-BP-ANN models) with swarm size of 10, acceleration factors c_1 = 1.75/1.5, c_2 = 1.75/2.5, weight of inertia ω = 0.4 and using 10 nodes achieved the best mapping or modeling of input–output correlation for the considered

membrane-based desalination system. The presented combined experimental and computational investigation paves the way for the study and development and modeling of similar novel TFC membrane materials for desalination and inherent process optimization.

Acknowledgments

The first author would like to thank the Ministry of Human Resource Development (MHRD), Government of India for providing research scholarship for executing the research work and also to Membrane Science and Separation Technology Division, Central Salt and Marine Chemicals Research Institute Bhavnagar, Gujarat, India for offering help with the experimental setup.

References

[1] M. Qasim, M. Badrelzaman, N.N. Darwish, N.A. Darwish, Reverse osmosis desalination: a state-of-the-art review, Desalination, 459 (2019) 59–104.
[2] M.A. Abdelkareem, M. El Haj Assad, E.T. Sayed, B. Soudan, Recent progress in the use of renewable energy sources to power water desalination plants, Desalination, 435 (2018) 97–113.
[3] S.S. Shenvi, A.M. Isloor, A.F. Ismail, A review on RO membrane technology: developments and challenges, Desalination, 368 (2015) 10–26.
[4] R. Mahadeva, G. Manik, O.P. Verma, S. Sinha, Modelling and simulation of desalination process using artificial neural network: a review, Desal. Water Treat., 122 (2018) 351–364.
[5] R. Mehta, H. Brahmbhatt, M. Mukherjee, A. Bhattacharya, Tuning separation behavior of tailor-made thin film poly(piperazine-amide) composite membranes for pesticides and salts from water, Desalination, 404 (2017) 280–290.
[6] R.J. Petersen, Composite reverse osmosis and nanofiltration membranes, J. Membr. Sci., 83 (1993) 81–150.
[7] R. Lo, A. Bhattacharya, B. Ganguly, Probing the selective salt rejection behavior of thin film composite membranes: a DFT study, J. Membr. Sci., 436 (2013) 90–96.
[8] R. Mehta, H. Brahmbhatt, N.K. Saha, A. Bhattacharya, Removal of substituted phenyl urea pesticides by reverse osmosis membranes: laboratory scale study for field water application, Desalination, 358 (2015) 69–75.
[9] R. Mahadeva, G. Manik, A. Goel, N. Dhakal, A review of the artificial neural network based modelling and simulation approaches applied to optimize reverse osmosis desalination techniques, Desal. Water Treat., 156 (2019) 245–256.
[10] F.E. Ahmed, R. Hashaikeh, A. Diabat, N. Hilal, Mathematical and optimization modelling in desalination: State-of-the-art and future direction, Desalination, 469 (2019) 114092.
[11] M.E. El-Hawary, Artificial neural networks and possible applications to desalination, Desalination, 92 (1993) 125–147.
[12] H. Niemi, A. Bulsari, S. Palosaari, Simulation of membrane separation by neural networks, J. Membr. Sci., 102 (1995) 185–191.
[13] A. Al-Alawi, S. M Al-Alawi, S. M Islam, Predictive control of an integrated PV-diesel water and power supply system using an artificial neural network, Renewable Energy, 32 (2007) 1426–1439.
[14] E.S. Salami, M. Ehetshami, A. Karimi-Jashni, M. Salari, S. Nikbakht Sheibani, A. Ehteshami, A mathematical method and artificial neural network modeling to simulate osmosis membrane's performance, Modell. Earth Syst. Environ., 2 (2016) 1–11.
[15] P. Cabrera, J.A. Carta, J. González, G. Melián, Wind-driven SWRO desalination prototype with and without batteries: a performance simulation using machine learning models, Desalination, 435 (2018) 77–96.
[16] R. Mahadeva, G. Manik, O.P. Verma, A. Goel, S. Kumar, Modelling and Simulation of Reverse Osmosis System Using PSO-ANN Prediction Technique, in: Adv. Intell. Syst. Comput., Springer, 1053, 2020, pp. 1209–1219.
[17] A. Goel, G. Manik, R. Mahadeva, A Review of Parabolic Trough Collector and Its Modeling, in: Adv. Intell. Syst. Comput., Springer, 1053, 2020, pp. 803–813.
[18] L.T. Le, H. Nguyen, J. Dou, J. Zhou, A comparative study of PSO-ANN, GA-ANN, ICA-ANN, and ABC-ANN in estimating the heating load of buildings' energy efficiency for smart city planning, Appl. Sci., 9 (2019) 1–23.
[19] S. Al Aani, T. Bonny, S.W. Hasan, N. Hilal, Can machine language and artificial intelligence revolutionize process automation for water treatment and desalination?, Desalination, 458 (2019) 84–96.
[20] M.A. Ahmadi, R. Soleimani, A. Bahadori, A computational intelligence scheme for prediction equilibrium water dew point of natural gas in TEG dehydration systems, Fuel, 137 (2014) 145–154.
[21] J. Kennedy, E. Russell, Particle swarm optimization, Proc. IEEE Int. Conf., (1995) 1942–1948.
[22] R. Eberhart, J. Kennedy, A New Optimizer Using Particle Swarm Theory, Proc. Int. Symp. Micro Mach. Hum. Sci., (1995) 39–43.
[23] M. Clerc, J. Kennedy, The particle swarm-explosion, stability, and convergence in a multidimensional complex space, IEEE Trans. Evol. Comput., 6 (2002) 58–73.
[24] R.C. Eberthart, Y. Shi, Comparing Inertia Weights and Constriction Factors in Particle Swarm Optimization, IEEE, 2000, pp. 84–88.
[25] R. Mehta, H. Brahmbhatt, G. Bhojani, M. Mukherjee, A. Bhattacharya, Poly(piperizinamide) with copper ion composite membranes: application for mitigation of Hexaconazole from water and combat microbial contamination, J. Hazard. Mater., 376 (2019) 102–111.
[26] J.M.M. Peeters, J.P. Boom, M.H.V. Mulder, H. Strathmann, Retention measurements of nanofiltration membranes with electrolyte solutions, J. Membr. Sci., 145 (1998) 199–209.
[27] A.L. Ahmad, B.S. Ooi, A.W. Mohammad, J.P. Choudhury, Composite nanofiltration polyamide membrane: a study on the diamine ratio and its performance evaluation, Ind. Eng. Chem. Res., 43 (2004) 8074–8082.
[28] D.J. Armaghani, E.T. Mohamad, M.S. Narayanasamy, N. Narita, S. Yagiz, Development of hybrid intelligent models for predicting TBM penetration rate in hard rock condition, Tunn. Undergr. Sp. Technol., 63 (2017) 29–43.
[29] M. Khajeh, M. Kaykhaii, A. Sharafi, Application of PSO-artificial neural network and response surface methodology for removal of methylene blue using silver nanoparticles from water samples, J. Ind. Eng. Chem., 19 (2013) 1624–1630.
[30] M. Buyukyildiz, G. Tezel, V. Yilmaz, Estimation of the change in lake water level by artificial intelligence methods, Water Resour. Manage., 28 (2014) 4747–4763.
[31] M. Khajeh, A. Sarafraz-Yazdi, A.F. Moghadam, Modeling of solid-phase tea waste extraction for the removal of manganese and cobalt from water samples by using PSO-artificial neural network and response surface methodology, Arabian J. Chem., 10 (2017) S1663–S1673.
[32] K.W. Chau, Particle swarm optimization training algorithm for ANNs in stage prediction of Shing Mun River, J. Hydrol., 329 (2006) 363–367.
[33] S.V. Alavi Nezhad Khalil Abad, M. Yilmaz, D. Jahed Armaghani, A. Tugrul, Prediction of the durability of limestone aggregates using computational techniques, Neural Comput. Appl., 29 (2018) 423–433.
[34] Y. Mei, J. Yang, Y. Lu, F. Hao, D. Xu, H. Pan, J. Wang, BP–ANN model coupled with particle swarm optimization for the efficient prediction of 2-chlorophenol removal in an electro-oxidation system, Int. J. Environ. Res. Public Health., 16 (2019) 2454.
[35] A. Aryafar, R. Mikaeil, F. Doulati Ardejani, S. Shaffiee Haghshenas, A. Jafarpour, Application of non-linear regression and soft computing techniques for modeling process of pollutant adsorption from industrial wastewaters, J. Min. Environ., 10 (2019) 327–337.

Supporting information

Simulation results for event-2 for NaCl rejection with low flux (Memb-I) have been presented Figs. S1 and S2 to understand the model performance for NaCl separation.

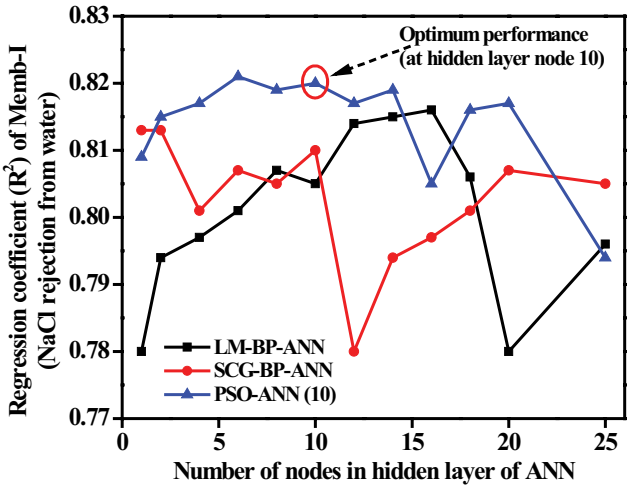

Fig. S1. Performance analysis of models LM-BP-ANN, SCG-BP-ANN, and PSO-ANN (swarm size 10) using regression coefficients (R^2) for Memb-I (low flux membrane) for NaCl rejection.

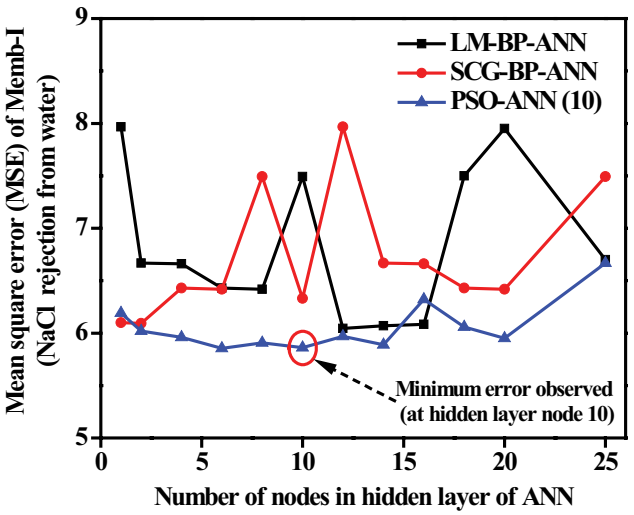

Fig. S2. Performance analysis of models LM-BP-ANN, SCG-BP-ANN, and PSO-ANN (swarm size 10) mean square error (MSE) for Memb-I (low flux membrane) for NaCl rejection.